

# Emergence of Exotic Spin Texture in Supramolecular Metal Complexes on a 2D Superconductor

Viliam Vaňo<sup>1</sup>, Stefano Reale<sup>2,3,4</sup>, Orlando J. Silveira<sup>1</sup>, Danilo Longo<sup>5</sup>, Mohammad Amini<sup>1</sup>, Massine Kelai,<sup>2,3</sup> Jaehyun Lee,<sup>2,6</sup> Atte Martikainen<sup>6</sup>, Shawulienu Kezilebieke<sup>8</sup>, Adam S. Foster<sup>1,9</sup>, Jose L. Lado<sup>10</sup>,  
Fabio Donati<sup>2,6,\*</sup>, Peter Liljeroth<sup>1,†</sup>, and Linghao Yan<sup>10,1,‡</sup>

<sup>1</sup>Department of Applied Physics, Aalto University, FI-00076 Aalto, Finland

<sup>2</sup>Center for Quantum Nanoscience (QNS), Institute for Basic Science (IBS), Seoul 03760, Republic of Korea

<sup>3</sup>Ewha Womans University, Seoul 03760, Republic of Korea

<sup>4</sup>Department of Energy, Politecnico di Milano, Milano 20133, Italy

<sup>5</sup>CIC nanoGUNE-BRTA, 20018 Donostia-San Sebastián, Spain

<sup>6</sup>Department of Physics, Ewha Womans University, Seoul 03760, Republic of Korea

<sup>7</sup>Department of Physics, P.O. Box 4, FI-00014 University of Helsinki, Finland

<sup>8</sup>Department of Physics, Department of Chemistry and Nanoscience Center, University of Jyväskylä, FI-40014 University of Jyväskylä, Finland

<sup>9</sup>WPI Nano Life Science Institute (WPI-NanoLSI), Kanazawa University, Kakuma-machi, Kanazawa 920-1192, Japan

<sup>10</sup>Institute of Functional Nano and Soft Materials (FUNSOM),

Jiangsu Key Laboratory for Carbon-Based Functional Materials and Devices,

Joint International Research Laboratory of Carbon-Based Functional Materials and Devices,

Soochow University, Suzhou 215123, China



(Received 29 November 2023; accepted 18 October 2024; published 6 December 2024)

Designer heterostructures have offered a very powerful strategy to create exotic superconducting states by combining magnetism and superconductivity. In this Letter, we use a heterostructure platform combining supramolecular metal complexes (SMCs) with a quasi-2D van der Waals superconductor NbSe<sub>2</sub>. Our scanning tunneling microscopy measurements demonstrate the emergence of Yu-Shiba-Rusinov bands arising from the interaction between the SMC magnetism and the NbSe<sub>2</sub> superconductivity. Using x-ray absorption spectroscopy and x-ray magnetic circular dichroism measurements, we show the presence of antiferromagnetic coupling between the SMC units. These result in the emergence of an unconventional 3 × 3 reconstruction in the magnetic ground state that is directly reflected in real space modulation of the Yu-Shiba-Rusinov bands. The combination of flexible molecular building blocks, frustrated magnetic textures, and superconductivity in heterostructures establishes a fertile starting point to fabricating tunable quantum materials, including unconventional superconductors and quantum spin liquids.

DOI: 10.1103/PhysRevLett.133.236203

Supramolecular metal complexes (SMCs) are a highly versatile class of metal-organic materials that combine flexible design, widely tuneable properties, and facile access to large scale structures via molecular self-assembly [1]. The ability to tune the lattice geometry, the magnetism and spin-orbit coupling arising from the metal atoms within these complexes, along with the diverse interactions with the substrate, has led to the prediction of a multitude of extraordinary electronic properties exhibited by SMCs [2,3]. Only a handful of these effects has been realized in practice, including the manifestation of magnetic properties [4,5], surface-state engineering [6], and the realization of structures potentially hosting topologically nontrivial band structures [7].

While SMCs can host intrinsic exotic states, creating heterostructures with proximity effects offers even more possibilities. For example, combining magnetic impurities with superconductivity can give rise to Yu-Shiba-Rusinov (YSR) states [8–10]. Arranging such impurities in 1D and 2D lattices together with a suitable magnetic texture and spin-orbit interactions provides a route to various artificial topological superconducting states [11–19]. Even though YSR bands have been successfully achieved in assemblies of individual magnetic atoms, and with inorganic chains and layers [19–24], the emergence of YSR bands in molecular systems still remains elusive [25–28]. The downside of this approach is that molecular systems on typical bulk superconducting substrates combine the large lattice constants of SMCs with small YSR orbitals. This leads to very limited overlap between the YSR states, hindering the potential creation of YSR bands. In addition, magnetic coupling between the SMC building blocks is typically small.

\*Contact author: donati.fabio@qns.science

†Contact author: peter.liljeroth@aalto.fi

‡Contact author: lhyan@suda.edu.cn

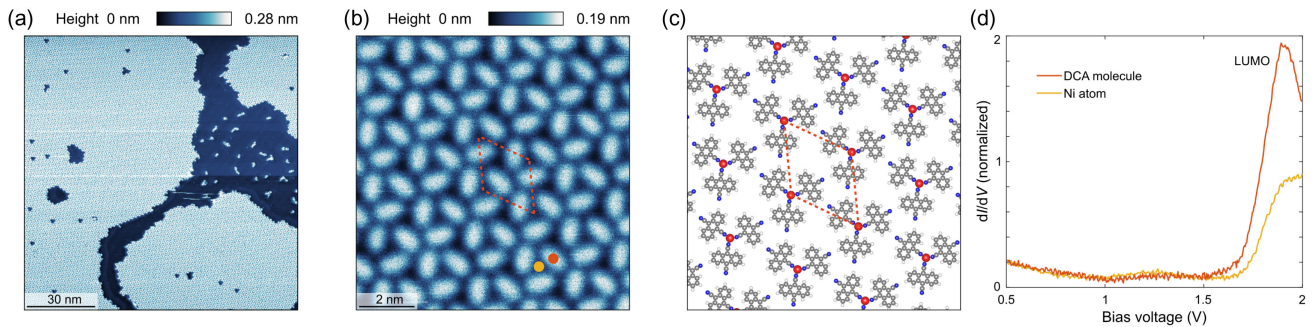


FIG. 1. Magnetic NiDCA<sub>3</sub> SMC on superconducting NbSe<sub>2</sub>. (a),(b) Large area STM image [(a)  $V = 1.73$  V,  $I = 10$  pA] and small area STM image [(b)  $V = 1$  V,  $I = 5$  pA] of NiDCA<sub>3</sub> SMC on NbSe<sub>2</sub>. (c) DFT calculated structure of the NiDCA<sub>3</sub> SMC on the NbSe<sub>2</sub> substrate (substrate atoms not shown). (d)  $dI/dV$  spectra measured on top of the DCA molecule (orange) and Ni atom (yellow) within the NiDCA<sub>3</sub> SMC.

NbSe<sub>2</sub> has been shown to host YSR states with spatially extended orbitals due to its quasi-2D character [29–31]. We demonstrate that this allows for a significant overlap of the YSR states in SMC-NbSe<sub>2</sub> heterostructures resulting in the formation of robust YSR bands. Furthermore, we show the presence of antiferromagnetic coupling within the SMC layer by synchrotron-based x-ray absorption spectroscopy (XAS) and magnetic circular dichroism (XMCD). Together with the triangular SMC lattice, this results in magnetic frustration giving rise to an unconventional  $3 \times 3$  reconstruction in the magnetic ground state. This modulation is directly reflected in the local density of states (LDOS) of the YSR bands that we probe via scanning tunneling microscopy (STM) and scanning tunneling spectroscopy. The successful synthesis of magnetically coupled SMC on NbSe<sub>2</sub> and the formation of YSR bands thus provides an archetypal platform for engineering unconventional quantum phases in SMC-superconductor hybrid systems.

*Heterostructure of NiDCA<sub>3</sub> on NbSe<sub>2</sub>*—The STM image in Fig. 1(a) shows the results of the growth of a single-layer NiDCA<sub>3</sub> (DCA = dicyanoanthracene) SMC on NbSe<sub>2</sub> (details of the sample preparation are given in the Supplemental Material (SM) [32]). The bright areas are self-assembled SMC islands extending over tens of nanometers, with smaller size SMC clusters randomly distributed between them. A smaller area STM image [Fig. 1(b)] reveals the triangular lattice of the SMC, which has the structure matching the density functional theory (DFT) calculations shown in Fig. 1(c). The building unit of the SMC consists of three DCA molecules surrounding a Ni atom, forming a NiDCA<sub>3</sub> single complex arranged in a triangular lattice. This metal coordination is similar to the earlier results on Co-DCA and Cu-DCA networks on graphene and NbSe<sub>2</sub> and in a stark contrast with the close-packed assembly of pure DCA molecules on NbSe<sub>2</sub> [33,61,62]. The magnetic Ni atoms create a triangular lattice of magnetic impurities on the superconducting NbSe<sub>2</sub> substrate [Fig. 1(c)], with an experimentally determined lattice constant of 2.03 nm that matches the value of 2.07 nm calculated by DFT [32]. The  $dI/dV$

spectra taken on top of Ni atom and DCA molecules show a broad peak between 1.5 and 2 V [Fig. 1(d)], representing the typical metal-ligand bonding orbital features formed in the single complex (see Fig. S1 in the SM) [33,34].

*Emergence of Yu-Shiba-Rusinov bands*—A single magnetic impurity on top of a superconductor induces a pair of YSR states inside the superconducting gap [8–10,21]. Analogous to the electronic lattice, the overlap of YSR states leads to their hybridization and thus to the formation of YSR bands. These appear as broad features in the spectral function rather than the sharp peaks stemming from single states. We investigated this using STM with a superconducting NbSe<sub>2</sub> tip that improves the energy resolution of the experiment and, more importantly, the stability of the measurements on the molecular assemblies [32]. Our experimental observations on SMCs on NbSe<sub>2</sub> confirm the expected transition from single YSR states to YSR bands: when an isolated single complex is positioned on NbSe<sub>2</sub> [Fig. 2(a)], two sharp peaks appear in the tunneling spectroscopy symmetrically around the Fermi level [Fig. 2(b)]. As these single complexes form a SMC lattice [Fig. 2(c)], the sharp peaks in the tunneling spectrum become broader and weaker in intensity [Fig. 2(d)]. This is a sign of strong hybridization and a band formation, which is enabled by the large spatial extent of YSR states of NbSe<sub>2</sub> [29–31] and leads to a significant overlap of these states between neighboring single complexes. Another sign of YSR band formation, as we will show in the following, is that there is a strong YSR LDOS across the whole unit cell of the SMC. Alternatively, the observed change in the YSR states could be due to the change in the effective temperature of the instrument or due to Pauli depairing. Both of these scenarios lead to changes in the spectroscopy of the superconducting gap, which we do not observe.

One of the advantages of our work, stemming from the large unit cell and extended YSR orbitals, is the further insight into spatial behavior of the YSR bands when probed by STM. This can reveal information about the orbital nature of the electronic state that induces the YSR state. While numerous studies have reported this for coupled

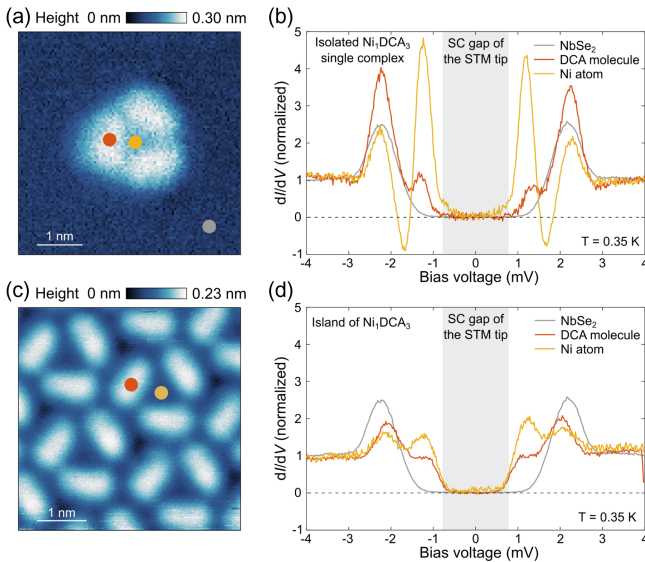


FIG. 2. Evolution from a single magnetic impurity to a lattice of magnetic impurities. (a) STM image of isolated NiDCA<sub>3</sub> single complex ( $V = 1$  V and  $I = 5$  pA). (b)  $dI/dV$  spectra measured with a superconducting tip on NbSe<sub>2</sub> (gray) and on Ni atom (yellow) and DCA molecule (orange) of the isolated NiDCA<sub>3</sub>, single complex. (c) STM image of NiDCA<sub>3</sub> SMC on NbSe<sub>2</sub> ( $V = 1$  V and  $I = 10$  pA). (d)  $dI/dV$  spectra measured with superconducting NbSe<sub>2</sub> tip on NbSe<sub>2</sub> (gray) and on the Ni (yellow) and DCA (orange) within the NiDCA<sub>3</sub> SMC.

YSR dimers and chains, research efforts focused on 2D YSR lattices remain notably limited [23,24]. The LDOS map in Fig. 3(b) visualizes the YSR band, which was measured on the area shown in Fig. 3(a). The intensity of the YSR bands is particularly concentrated around the central Ni atom of each single complex, where DFT finds maximal spin density. However, due to the remarkable spatial extent of the YSR states, a pronounced intensity pattern is visible across the whole unit cell even where the spin density vanishes [Fig. 3(c)]. The additional long-range modulation of the YSR band occurring over several unit cells shown in Fig. 3(a) is due to a magnetic ground state (see below).

*Magnetism of Ni atoms from XAS and XMCD*—To gain insight into the electronic configuration of the Ni atoms in the SMC, XAS and XMCD measurements were conducted at the DEIMOS beamline of the SOLEIL synchrotron [32]. Figure 3(d) shows the spectra collected at the  $L_{2,3}$  edges of Ni exhibiting a characteristic  $3d^8$  line shape [63]. The large XMCD signal indicates a high spin configuration with a triplet  $S = 1$  ground state. Angular-dependent XAS and XMCD measurements reveal a weak magnetic anisotropy, with a greater magnetization along the out-of-plane direction [32]. To quantitatively analyze the magnetic state of the Ni atoms, we performed a fitting procedure using simulated spectra based on atomic multiplet calculations. The calculations considered a Ni  $3d^8$  configuration, accounting for intra-atomic electron-electron interactions, spin-orbit

coupling, crystal field effects within the  $C_{3v}$  symmetry, and an external magnetic field [32]. The result of the fit, overlaid to the experiment in Fig. 3(d), supports the inferred  $3d^8$  configuration with a  $S = 1$  triplet ground state and allows quantifying a value for the magnetic anisotropy of about 0.1 meV. While the multiplet model nicely reproduces the shape of both XAS and XMCD spectra, the amplitude of the XMCD signal appears to be slightly overestimated. As discussed in the following section, the inclusion of antiferromagnetic interactions between the Ni atoms enables a comprehensive reproduction of the XMCD amplitude at all magnetic fields and temperatures. Additionally, we computed the projected density of states (PDOS) for the Ni  $d$  orbitals [Fig. 3(e)] by DFT and determined the orbital occupation of  $3d^8$  magnetic state for the Ni atoms based on inputs from x-ray absorption spectroscopy [Fig. 3(d)]. These results demonstrate that the studied SMC realizes a  $S = 1$  lattice.

To unravel the nature and strength of the magnetic interactions in the SMC, we acquired magnetization loops by measuring the XMCD signal [Fig. 3(d), down], while sweeping the applied magnetic field over a range between  $-6$  and  $+6$  T, and at temperatures from 2 to 50 K. The curve acquired at 2 K shown in Fig. 4(a) shows a smooth reversible loop, with no hysteresis or magnetization jumps between the backward and forward branch indicating the absence of stable magnetic structures at that temperature. However, the amplitude and slope of the curve are lower than the expected values of a  $S = 1$  Brillouin function at  $T = 2.0$  K (black solid line). Including the full multiplet structure (red solid line) only marginally improves the discrepancy between experiment and theory. The same type of discrepancy appears in the magnetic susceptibility extracted from the magnetization loops as a function of temperature [see Fig. 4(b)], with both  $S = 1$  Brillouin and full multiplet model not capturing the experimental trend. The model improves remarkably by assuming the presence of antiferromagnetic interactions through  $n$  nearest-neighbor pairwise exchange  $J^{\text{ex}}$  resulting in a Curie-Weiss temperature  $T_{\text{CW}} = -[S(S+1)/3k_B]nJ^{\text{ex}}$  [64], which we take as a free parameter of the fit (green solid line). The combination of multiplet calculations and the just mentioned antiferromagnetic interaction provides an excellent agreement with the experiment for a  $T_{\text{CW}} = -2.5 \pm 0.4$  K, which corresponds to an exchange energy of about 0.2 meV. This indicates that the exchange interaction between the Ni atoms dominates over the magnetic anisotropy. The relation between  $T_{\text{CW}}$  and the ordering Néel temperature  $T_N$  depends on the geometry of the spin lattice and on the neighbor order contributing to the magnetic coupling. For the case of a frustrated triangular-type lattice where only the first nearest neighbors are considered [64],  $T_N = -T_{\text{CW}}/2 = 1.2 \pm 0.2$  K, i.e., lower than the base temperature for XMCD measurements, in line with what was observed above. The low Curie-Weiss and

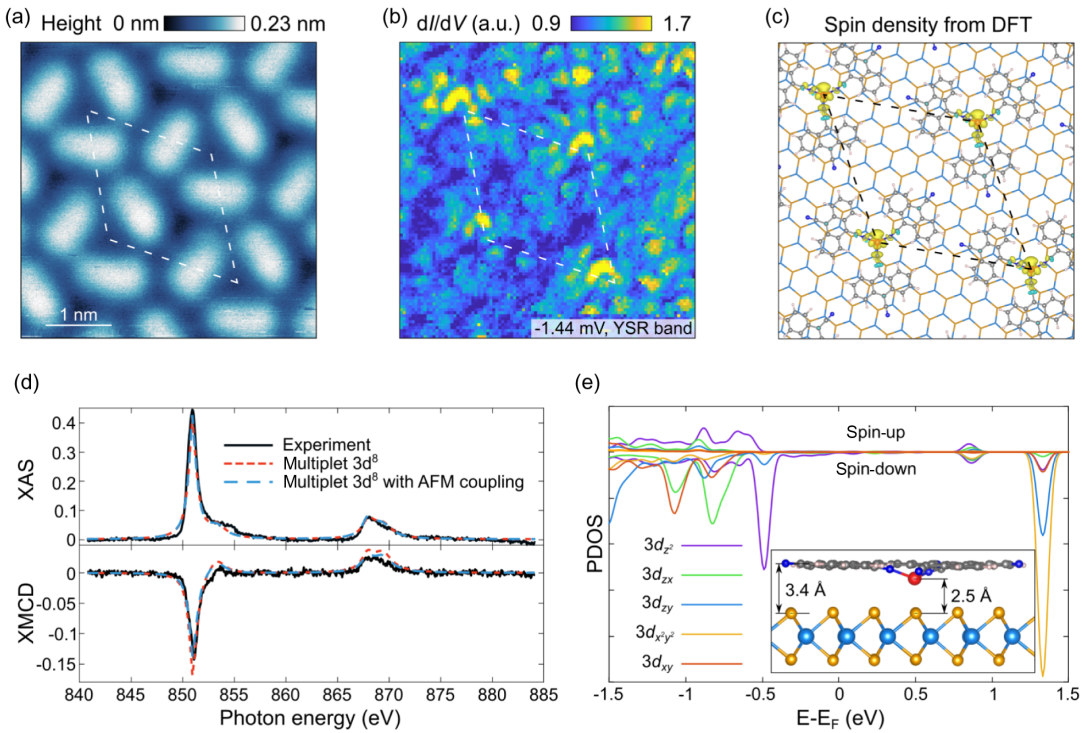


FIG. 3. Spatial distribution of the YSR bands and electronic configuration of the Ni. (a) STM image of NiDCA<sub>3</sub> SMC on NbSe<sub>2</sub> ( $V = 1$  V and  $I = 10$  pA). (b)  $dI/dV$  map of the area shown in (a) at  $V = -1.44$  mV, corresponding to the energy of the YSR band (feedback parameters  $V = 4$  mV,  $I = 80$  pA, and  $V_{\text{mod}} = 100$   $\mu$ V). (c) Spatial distribution of the spin density of NiDCA<sub>3</sub> on NbSe<sub>2</sub>, calculated by DFT. (d) XAS and corresponding XMCD of the NiDCA<sub>3</sub> on NbSe<sub>2</sub> at the Ni  $L_{2,3}$  edges, acquired at normal incidence. Experiments (blue lines) are compared with multiplet calculations performed for a  $3d^8$  configuration neglecting (green dashed lines) or including (red dashed lines) a magnetic coupling among the Ni centers; see text for more details ( $T_{\text{sample}} = 1.9$  K, magnetic field  $B = 6.0$  T). (e) PDOS of Ni 3d orbitals within the NiDCA<sub>3</sub> SMC, calculated by DFT. The structure is shown in the inset, where the light blue spheres correspond to Nb atoms, yellow to Se atoms, red to Ni atoms, grey to C atoms, blue to N atoms, and white to H atoms.

Néel temperatures are consistent with the relatively large distances and absence of chemical bonds between the single complexes.

*3 × 3 magnetic order from STM measurements*—The combination of antiferromagnetic coupling and a frustrated triangular lattice can give rise to exotic magnetic ground states, such as a quantum spin liquid or 120° Néel order. To determine the ground state of the SMC, we map the periodicity of the YSR signal with STM at a temperature of 350 mK, i.e., below the expected ordering temperature of 1.25 K. The magnetic order can be imprinted in the YSR states as the energy and density distribution of YSR states depend on the relative angle between magnetic moments. The STM results in Figs. 4(c),(d) show  $dI/dV(\vec{q}, V)$ , a fast Fourier transform of a LDOS map at the energy of the YSR bands. The main features here are the Bragg peaks (red circles) and  $3 \times 3$  peaks (blue circles). Within the  $\vec{q}$  resolution of the  $dI/dV(\vec{q}, V)$ , our data suggests that the  $3 \times 3$  peaks are aligned with the Bragg peaks. Upon applying an external magnetic field of  $B = 4$  T, at which there is no observable superconducting gap in the tunneling spectroscopy [65], the Bragg peaks remain while the  $3 \times 3$  peaks disappear. This suggests that the  $3 \times 3$  peaks are

connected to the YSR bands that rely on superconductivity. Alternatively, a magnetic field of 4 T could align the spins into a ferromagnetic structure, destroying the  $3 \times 3$  supercell. Both of these explanations support the magnetic ground state reconstruction that is imprinted in the YSR bands. The  $3 \times 3$  supercell of YSR bands could also arise due to a moiré pattern, where the registry of Ni atoms with respect to Se atoms of NbSe<sub>2</sub> repeats on a  $3 \times 3$  supercell. Similarly, the pattern could appear due to a repeating registry between the Ni atoms and  $3 \times 3$  charge density wave of NbSe<sub>2</sub>. However, our analysis shows that these cases can be ruled out [32]. Therefore, the supercell is likely to arise from a  $3 \times 3$  magnetic order of the Ni atoms within the SMC.

Besides, there are additional peaks in the  $dI/dV(\vec{q}, V)$ , and even though we cannot determine their exact origin at this point, they are not related to the superconducting state as they appear the same at 0 T and 4 T.

*Theoretical modeling*—To explain how the magnetic reconstruction can be observed in the STM signal, we present in Figs. 4(e)–(g) model calculations for a system with magnetic reconstruction shown in Fig. 4(e). The magnetic ordering induces an exchange coupling in the

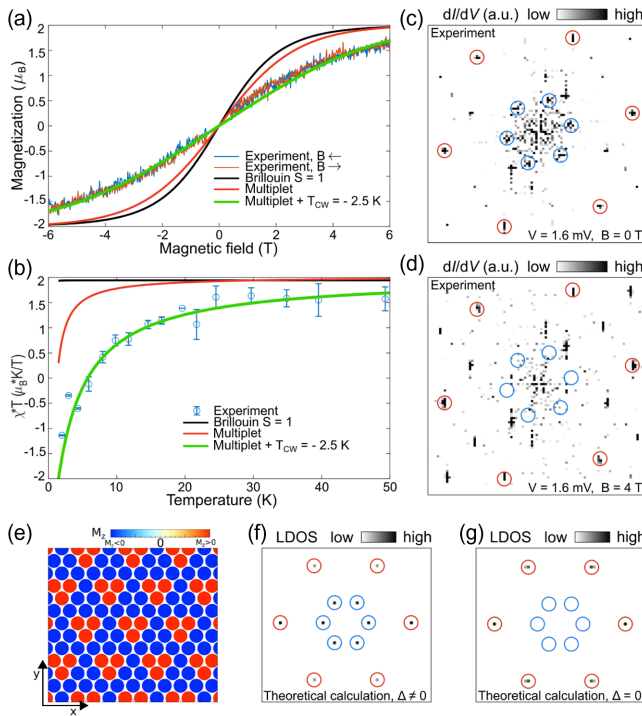


FIG. 4. Magnetic order of the NiDCA<sub>3</sub> SMC. (a) Hysteresis curve at  $T = 2.0$  K obtained by measuring the XMCD signal while sweeping the magnetic field. Brillouin curve for  $S = 1$  (solid black line), equilibrium magnetization from the multiplet model neglecting (red solid line), and including an antiferromagnetic interaction with a Curie-Weiss temperature  $T_{CW} = -2.5$  K (green solid line) are shown for comparison. (b) Temperature dependence of the susceptibility obtained from hysteresis curves at various temperatures and comparison with the related models. Data shown in (a) and (b) were acquired at normal incidence. (c),(d)  $dI/dV(\vec{q}, V)$  measured at the energy of the YSR bands ( $V = 1.6$  mV) at 0 Tesla (c) and 4 Tesla (d), acquired at  $T = 350$  mK. Red circles correspond to the Bragg peaks and blue circles to  $3 \times 3$  peaks related to the antiferromagnetic order. (e) Illustration of the  $3 \times 3$  Ising-like magnetic ground state consistent with our observations. (f) Simulated LDOS( $\vec{q}$ ) of the in-gap Yu-Shiba-Rusinov states, allowing the imaging of the magnetic reconstruction in the YSR band structure. (g) In the absence of superconductivity, the additional peaks are not observed in the LDOS( $\vec{q}$ ).

underlying substrate, leading to a modulated exchange profile [32]. This phenomenology is illustrated here with an Ising-like  $3 \times 3$  magnetic configuration, realizing a minimal ground state with strong out-of-plane anisotropy. In the case of weaker out-of-plane anisotropy, noncollinear configurations featuring  $3 \times 3$  periodicity would be consistent with our observations as analyzed in the SM [32]. The magnetic modulation translates into the modulation of the energy of YSR states, reflecting the broken translational symmetry of the magnetic structure. The energy modulation of the YSR states can be visualized as a LDOS modulation at an in-gap energy featuring YSR modes [Fig. 4(f)]. In stark contrast, in the absence of

superconductivity or a magnetic superstructure, no additional peaks are observed in the fast Fourier transform of the  $dI/dV(\vec{q}, V)$  signal [Fig. 4(g); see SM [32] for details]. While the STM experiments do not directly probe the magnetism of the SMC, the interplay between magnetism and superconductivity translates the magnetic texture into a spatial modulation of the YSR bands that can be seen in the STM experiments. This allows visualizing frustrated magnetic orders directly in STM and scanning tunneling spectroscopy experiments.

**Conclusions**—We have successfully synthesized a magnetic SMC on a quasi-2D superconductor NbSe<sub>2</sub>, and investigated its electronic and magnetic properties using STM and XMCD. The STM experiments demonstrate that this heterostructure of a magnetic lattice and a superconductor leads to the emergence of YSR bands spanning the entire unit cell of the SMC. Furthermore, combining XMCD and STM results, we discovered an exotic  $3 \times 3$  antiferromagnetic order of the SMC. We use STM in a novel and unique way to extract information about the spin texture of the system, which is imprinted in the YSR bands. These results open up an extremely tunable path toward realizing novel quantum phases, such as topological superconductivity or quantum spin liquids using SMC-superconductor heterostructures. Here, the tunability stems from the choice of metal atoms, molecules, and the substrate, which allows for a combination of different ingredients for designing a wide range of physical systems.

**Acknowledgments**—This research made use of the Aalto Nanomicroscopy Center (Aalto NMC) facilities and was supported by the European Research Council (ERC-2017-AdG No. 788185 “Artificial Designer Materials”) and Research Council of Finland (Academy professor funding No. 318995 and No. 320555, Academy research fellow No. 331342, No. 336243 and No. 338478 and No. 346654). L. Y. acknowledges support from the Jiangsu Specially-Appointed Professors Program, Natural Science Foundation of Jiangsu Province (Grant No. BK20230474), Suzhou Key Laboratory of Surface and Interface Intelligent Matter (Grant No. SZS2022011), Gusu Innovation and Entrepreneurship Talent Program—Major Innovation Team (ZXD2023002), Suzhou Key Laboratory of Functional Nano and Soft Materials, Collaborative Innovation Center of Suzhou Nano Science and Technology, and the 111 Project. Computing resources from the Aalto Science-IT project and CSC, Helsinki are gratefully acknowledged. A. S. F has been supported by the World Premier International Research Center Initiative (WPI), MEXT, Japan. S. R, M. K, J. L, and F. D. acknowledge support from the Institute for Basic Science under Grant No. IBS-R027-D1. D. L. acknowledges support from the MSCA project (Project No. 101064332). We are grateful to Fadi Choueikani for assistance with XAS and XMCD experiments and to the SOLEIL staff for smoothly

running the facility. The authors would like to thank Bernard Muller for his significant contribution to the construction of DEIMOS beamline (design and engineering) and Florian Leduc for his support. The MBE chamber used during the XAS/XCMD experiment on DEIMOS has been funded by the Agence National de la Recherche, Grant No. ANR-05-NANO-073.

**Data availability**—The DFT and multiplet computational data and metadata are freely available under a CC BY 4.0 license on the following link [66]. The low energy model code is available on [67]. Experimental data is available upon reasonable request.

[1] L. Dong, Z. Gao, and N. Lin, Self-assembly of metal-organic coordination structures on surfaces, *Prog. Surf. Sci.* **91**, 101 (2016).

[2] M. A. Springer, T.-J. Liu, A. Kuc, and T. Heine, Topological two-dimensional polymers, *Chem. Soc. Rev.* **49**, 2007 (2020).

[3] W. Jiang, X. Ni, and F. Liu, Exotic topological bands and quantum states in metal-organic and covalent-organic frameworks, *Acc. Chem. Res.* **54**, 416 (2021).

[4] P. Gambardella, S. Stepanow, A. Dmitriev, J. Honolka, F. M. D. Groot, M. Lingenfelder, S. S. Gupta, D. D. Sarma, P. Bencok, S. Stanescu, S. Clair, S. Pons, N. Lin, A. P. Seitsonen, H. Brune, J. V. Barth, and K. Kern, Supramolecular control of the magnetic anisotropy in two-dimensional high-spin Fe arrays at a metal interface, *Nat. Mater.* **8**, 189 (2009).

[5] J. Girovsky, J. Nowakowski, M. E. Ali, M. Baljozovic, H. R. Rossmann, T. Nijs, E. A. Aeby, S. Nowakowska, D. Siewert, G. Srivastava, C. Wäckerlin, J. Dreiser, S. Decurtins, S.-X. Liu, P. M. Oppeneer, T. A. Jung, and N. Ballav, Long-range ferrimagnetic order in a two-dimensional supramolecular Kondo lattice, *Nat. Commun.* **8**, 15388 (2017).

[6] I. Piquero-Zulaica, J. Lobo-Checa, Z. M. A. El-Fattah, J. E. Ortega, F. Klappenberger, W. Auwärter, and J. V. Barth, Engineering quantum states and electronic landscapes through surface molecular nanoarchitectures, *Rev. Mod. Phys.* **94**, 045008 (2022).

[7] Z. Gao, C. H. Hsu, J. Liu, F. C. Chuang, R. Zhang, B. Xia, H. Xu, L. Huang, Q. Jin, P. N. Liu, and N. Lin, Synthesis and characterization of a single-layer conjugated metal-organic structure featuring a non-trivial topological gap, *Nanoscale* **11**, 878 (2019).

[8] L. Yu, Bound state in superconductors with paramagnetic impurities, *Acta Phys. Sin.* **21**, 75 (1965).

[9] H. Shiba, Classical spins in superconductors, *Prog. Theor. Phys.* **40**, 435 (1968).

[10] A. I. Rusinov, On the theory of gapless superconductivity in alloys containing paramagnetic impurities, Sov. Phys. JETP **29**, 1101 (1969), <http://jetp.ras.ru/cgi-bin/e/index/e/29/6/p1101?a=list>.

[11] S. Nadj-Perge, I. K. Drozdov, J. Li, H. Chen, S. Jeon, J. Seo, A. H. MacDonald, B. A. Bernevig, and A. Yazdani, Observation of Majorana fermions in ferromagnetic atomic chains on a superconductor, *Science* **346**, 602 (2014).

[12] J. Röntynen and T. Ojanen, Topological superconductivity and high Chern numbers in 2D ferromagnetic Shiba lattices, *Phys. Rev. Lett.* **114**, 236803 (2015).

[13] J. Li, T. Neupert, Z. Wang, A. H. MacDonald, A. Yazdani, and B. Andrei Bernevig, Two-dimensional chiral topological superconductivity in Shiba lattices, *Nat. Commun.* **7**, 12297 (2016).

[14] Y. Lu, W. Y. He, D. H. Xu, N. Lin, and K. T. Law, Platform for engineering topological superconductors: Superlattices on Rashba superconductors, *Phys. Rev. B* **94**, 024507 (2016).

[15] S. Rachel, E. Mascot, S. Cocklin, M. Vojta, and D. K. Morr, Quantized charge transport in chiral Majorana edge modes, *Phys. Rev. B* **96**, 205131 (2017).

[16] K. Pöyhönen, I. Sahlberg, A. Westström, and T. Ojanen, Amorphous topological superconductivity in a Shiba glass, *Nat. Commun.* **9**, 2103 (2018).

[17] L. Schneider, P. Beck, J. Neuhaus-Steinmetz, L. Rózsa, T. Posske, J. Wiebe, and R. Wiesendanger, Precursors of Majorana modes and their length-dependent energy oscillations probed at both ends of atomic Shiba chains, *Nat. Nanotechnol.* **17**, 384 (2022).

[18] K. Flensberg, F. von Oppen, and A. Stern, Engineered platforms for topological superconductivity and Majorana zero modes, *Nat. Rev. Mater.* **6**, 944 (2021).

[19] A. Yazdani, F. von Oppen, B. I. Halperin, and A. Yacoby, Hunting for Majoranas, *Science* **380**, eade0850 (2023).

[20] S.-H. Ji, T. Zhang, Y.-S. Fu, X. Chen, J.-F. Jia, Q.-K. Xue, and X.-C. Ma, Application of magnetic atom induced bound states in superconducting gap for chemical identification of single magnetic atoms, *Appl. Phys. Lett.* **96**, 073113 (2010).

[21] B. W. Heinrich, J. I. Pascual, and K. J. Franke, Single magnetic adsorbates on s-wave superconductors, *Prog. Surf. Sci.* **93**, 1 (2018).

[22] L. Schneider, P. Beck, L. Rózsa, T. Posske, J. Wiebe, and R. Wiesendanger, Probing the topologically trivial nature of end states in antiferromagnetic atomic chains on superconductors, *Nat. Commun.* **14**, 2742 (2023).

[23] M. Bazarnik, R. Lo Conte, E. Mascot, K. von Bergmann, D. K. Morr, and R. Wiesendanger, Antiferromagnetism-driven two-dimensional topological nodal-point superconductivity, *Nat. Commun.* **14**, 614 (2023).

[24] M. O. Soldini, F. Küster, G. Wagner, S. Das, A. Aldarawsheh, R. Thomale, S. Lounis, S. S. P. Parkin, P. Sessi, and T. Neupert, Two-dimensional Shiba lattices as a possible platform for crystalline topological superconductivity, *Nat. Phys.* **19**, 1848 (2023).

[25] K. J. Franke, G. Schulze, and J. I. Pascual, Competition of superconducting phenomena and Kondo screening at the nanoscale, *Science* **332**, 940 (2011).

[26] N. Hatter, B. W. Heinrich, M. Ruby, J. I. Pascual, and K. J. Franke, Magnetic anisotropy in Shiba bound states across a quantum phase transition, *Nat. Commun.* **6**, 8988 (2015).

[27] C. Mier, B. Verlhac, L. Garnier, R. Robles, L. Limot, N. Lorente, and D. J. Choi, Superconducting scanning tunneling microscope tip to reveal sub-millielectronvolt magnetic energy variations on surfaces, *J. Phys. Chem. Lett.* **12**, 2983 (2021).

[28] L. Farinacci, G. Reecht, F. von Oppen, and K. J. Franke, Yu-Shiba-Rusinov bands in a self-assembled kagome lattice of magnetic molecules, *Nat. Commun.* **15**, 6474 (2024).

[29] G. C. Ménard, S. Guissart, C. Brun, S. Pons, V. S. Stolyarov, F. Debontridder, M. V. Leclerc, E. Janod, L. Cario, D. Roditchev, P. Simon, and T. Cren, Coherent long-range magnetic bound states in a superconductor, *Nat. Phys.* **11**, 1013 (2015).

[30] S. Kezilebieke, M. Dvorak, T. Ojanen, and P. Liljeroth, Coupled Yu-Shiba-Rusinov states in molecular dimers on  $\text{NbSe}_2$ , *Nano Lett.* **18**, 2311 (2018).

[31] E. Liebhaber, L. M. Rütten, G. Reecht, J. F. Steiner, S. Röhl, K. Rossnagel, F. von Oppen, and K. J. Franke, Quantum spins and hybridization in artificially-constructed chains of magnetic adatoms on a superconductor, *Nat. Commun.* **13**, 2160 (2022).

[32] See Supplemental Material at <http://link.aps.org/supplemental/10.1103/PhysRevLett.133.236203>, which includes Refs. [25,30,33–60], for experimental and computational methods, additional STM, tunneling spectroscopy, and x-ray spectroscopy results, discussion on the origin of the observed modulation of the YSR bands, and detailed description of the theoretical model.

[33] A. Kumar, K. Banerjee, A. S. Foster, and P. Liljeroth, Two-dimensional band structure in honeycomb metal-organic frameworks, *Nano Lett.* **18**, 5596 (2018).

[34] P. Liljeroth, I. Swart, S. Paavilainen, J. Repp, and G. Meyer, Single-molecule synthesis and characterization of metal-ligand complexes by low-temperature STM, *Nano Lett.* **10**, 2475 (2010).

[35] P. Ohresser, E. Otero, F. Choueikani, K. Chen, S. Stanescu, F. Deschamps, T. Moreno, F. Polack, B. Lagarde, J.-P. Daguerre, F. Marteau, F. Scheurer, L. Joly, J.-P. Kappler, B. Müller, O. Buna, and P. Sainctavit, DEIMOS: A beamline dedicated to dichroism measurements in the 350–2500 eV energy range, *Rev. Sci. Instrum.* **85**, 013106 (2014).

[36] L. Joly, E. Otero, F. Choueikani, F. Marteau, L. Chapuis, and P. Ohresser, Fast continuous energy scan with dynamic coupling of the monochromator and undulator at the DEIMOS beamline, *J. Synchrotron Radiat.* **21**, 502 (2014).

[37] L. Malavolti, M. Briganti, M. Hänze, G. Serrano, I. Cimatti, G. McMurtie, E. Otero, P. Ohresser, F. Totti, M. Mannini, R. Sessoli, and S. Loth, Tunable spin–superconductor coupling of spin 1/2 vanadyl phthalocyanine molecules, *Nano Lett.* **18**, 7955 (2018).

[38] G. Serrano, L. Poggini, G. Cucinotta, A. L. Sorrentino, N. Giacconi, B. Cortigiani, D. Longo, E. Otero, P. Sainctavit, A. Caneschi, M. Mannini, and R. Sessoli, Magnetic molecules as local sensors of topological hysteresis of superconductors, *Nat. Commun.* **13**, 3838 (2022).

[39] L. Poggini, A. L. Sorrentino, D. Ranieri, A. Calloni, F. Santanni, N. Giacconi, G. Cucinotta, E. Otero, D. Longo, B. Cortigiani, A. Caneschi, G. Bussetti, R. Sessoli, M. Mannini, and G. Serrano, Electronic and magnetic properties of a monolayer of VOTP molecules sublimated on Ag (100), *Adv. Phys. Res.* **3**, 2300121 (2024).

[40] M. W. Haverkort, Quanty for core level spectroscopy—excitons, resonances and band excitations in time and frequency domain, *J. Phys. Conf. Ser.* **712**, 012001 (2016).

[41] R. D. Cowan, *The Theory of Atomic Structure and Spectra* (University of California Press, Berkeley, 1981).

[42] M. O. Krause and J. H. Oliver, Natural widths of atomic K and L levels,  $\text{K}\alpha$  Xray lines and several KLL Auger lines, *J. Phys. Chem. Ref. Data* **8**, 329 (1979).

[43] P. Giannozzi *et al.*, Quantum Espresso: A modular and open-source software project for quantum simulations of materials, *J. Phys. Condens. Matter* **21**, 395502 (2009).

[44] S. Grimme, J. Antony, S. Ehrlich, and H. Krieg, A consistent and accurate *ab initio* parametrization of density functional dispersion correction (DFT-D) for the 94 elements H–Pu, *J. Chem. Phys.* **132**, 154104 (2010).

[45] A. M. Rappe, K. M. Rabe, E. Kaxiras, and J. D. Joannopoulos, Optimized pseudopotentials, *Phys. Rev. B* **41**, 1227 (1990).

[46] M. Cococcioni and S. de Gironcoli, Linear response approach to the calculation of the effective interaction parameters in the LDA + U method, *Phys. Rev. B* **71**, 035105 (2005).

[47] S. H. Pan, E. W. Hudson, and J. C. Davis, Vacuum tunneling of superconducting quasiparticles from atomically sharp scanning tunneling microscope tips, *Appl. Phys. Lett.* **73**, 2992 (1998).

[48] S.-H. Ji, T. Zhang, Y.-S. Fu, X. Chen, X.-C. Ma, J. Li, W.-H. Duan, J.-F. Jia, and Q.-K. Xue, High-resolution scanning tunneling spectroscopy of magnetic impurity induced bound states in the superconducting gap of Pb thin films, *Phys. Rev. Lett.* **100**, 226801 (2008).

[49] S. Gao, H. D. Rosales, F. A. Gómez Albaracín, V. Tsurkan, G. Kaur, T. Fennell, P. Steffens, M. Boehm, P. Čermák, A. Schneidewind, E. Ressouche, D. C. Cabra, C. Rüegg, and O. Zaharko, Fractional antiferromagnetic skyrmion lattice induced by anisotropic couplings, *Nature (London)* **586**, 37 (2020).

[50] I. Dzyaloshinsky, A thermodynamic theory of “weak” ferromagnetism of antiferromagnetics, *J. Phys. Chem. Solids* **4**, 241 (1958).

[51] T. Moriya, Anisotropic superexchange interaction and weak ferromagnetism, *Phys. Rev.* **120**, 91 (1960).

[52] A. Crépieux and C. Lacroix, Dzyaloshinsky–Moriya interactions induced by symmetry breaking at a surface, *J. Magn. Magn. Mater.* **182**, 341 (1998).

[53] A. Fert, V. Cros, and J. Sampaio, Skyrmions on the track, *Nat. Nanotechnol.* **8**, 152 (2013).

[54] S. Hayami and Y. Motome, Square skyrmion crystal in centrosymmetric itinerant magnets, *Phys. Rev. B* **103**, 024439 (2021).

[55] S. Paul, S. Haldar, S. von Malottki, and S. Heinze, Role of higher-order exchange interactions for skyrmion stability, *Nat. Commun.* **11**, 4756 (2020).

[56] S. Hayami, R. Ozawa, and Y. Motome, Effective bilinear-biquadratic model for noncoplanar ordering in itinerant magnets, *Phys. Rev. B* **95**, 224424 (2017).

[57] S. Okumura, S. Hayami, Y. Kato, and Y. Motome, Magnetic hedgehog lattices in noncentrosymmetric metals, *Phys. Rev. B* **101**, 144416 (2020).

[58] R. Ozawa, S. Hayami, and Y. Motome, Zero-field skyrmions with a high topological number in itinerant magnets, *Phys. Rev. Lett.* **118**, 147205 (2017).

[59] T. Okubo, S. Chung, and H. Kawamura, Multiple- $q$  states and the skyrmion lattice of the triangular-lattice Heisenberg antiferromagnet under magnetic fields, *Phys. Rev. Lett.* **108**, 017206 (2012).

[60] T. Kurumaji, T. Nakajima, M. Hirschberger, A. Kikkawa, Y. Yamasaki, H. Sagayama, H. Nakao, Y. Taguchi, T.-h. Arima, and Y. Tokura, Skyrmion lattice with a giant topological Hall effect in a frustrated triangular-lattice magnet, *Science* **365**, 914 (2019).

[61] L. Yan, O. J. Silveira, B. Alldritt, S. Kezilebieke, A. S. Foster, and P. Liljeroth, Two-dimensional metal–organic framework on superconducting  $\text{NbSe}_2$ , *ACS Nano* **15**, 17813 (2021).

[62] L. Yan, O. J. Silveira, B. Alldritt, O. Krejčí, A. S. Foster, and P. Liljeroth, Synthesis and local probe gating of a monolayer metal–organic framework, *Adv. Funct. Mater.* **31**, 2100519 (2021).

[63] C. Klewe, M. Meinert, A. Boehnke, K. Kuepper, E. Arenholz, A. Gupta, J.-M. Schmalhorst, T. Kuschel, and G. Reiss, Physical characteristics and cation distribution of  $\text{NiFe}_2\text{O}_4$  thin films with high resistivity prepared by reactive co-sputtering, *J. Appl. Phys.* **115**, 123903 (2014).

[64] D. C. Johnston, Magnetic susceptibility of collinear and noncollinear Heisenberg antiferromagnets, *Phys. Rev. Lett.* **109**, 077201 (2012).

[65] S. Kezilebieke, M. N. Huda, V. Vaňo, M. Aapro, S. C. Ganguli, O. J. Silveira, S. Głodzik, A. S. Foster, T. Ojanen, and P. Liljeroth, Topological superconductivity in a van der Waals heterostructure, *Nature (London)* **588**, 424 (2020).

[66] O. J. Silveira, S. Reale, L. Jaehyun, and F. Donati, Theoretical simulations for: Emergence of exotic spin texture in supramolecular metal complexes on a 2D superconductor [Data set]. Zenodo, 10.5281/zenodo.13969023.

[67] <https://github.com/joselado/pyqula>